PCCP

Accepted Manuscript

ROYAL SOCIETY OF CHEMISTRY

www.rsc.org/pccp

Synthesis of Silicon-Germanium Axial Nanowire Heterostructures in a Solvent Vapor Growth System using Indium and Tin Catalysts

*E. Mullane, H. Geaney, K. M. Ryan**

Materials and Surface Science Institute and Department of Chemical and Environmental Sciences, University of Limerick, Limerick, Ireland

*Author to whom correspondence should be addressed.

Abstract

Here we describe a relatively facile synthetic protocol for the formation of Si/Ge and Si/Ge/$Si_{1-x}Ge_x$ axial nanowire heterostructures. The wires are grown directly on substrates with an evaporated catalytic layer placed in the vapour zone of a high boiling point solvent with the silicon and germanium precursors injected as liquids sequentially. We show that these heterostructures can be formed using either indium or tin as the catalyst seeds which form *in-situ* during the thermal anneal. There is a direct correlation between growth time and segment length allowing good control over the wire composition. The formation of axial heterostructures of Si/Ge/$Si_{1-x}Ge_x$ nanowires using a triple injection is further discussed with the alloyed $Si_{1-x}Ge_x$ third component formed due to residual Ge precursor and its greater reactivity in comparison to silicon. It was found that the degree of tapering at each hetero-interface varied with both the catalyst type and composition of the NW. The report shows the versatility of the solvent vapour growth system for the formation of complex Si/Ge NW heterostructures.

Introduction

Si and Ge nanowires (NWs) are a widely studied material set which have shown promise in a range of important and diverse applications from next generation wrap around gate transistors to photovoltaic light harvesting antennae and lithium alloying battery anodes.[1-7] The ability to grow single crystal wires of defined diameters at the nanoscale allows their properties to be investigated as a function of size, providing greater insight into their suitability for next generation devices. As covalent network solids with high melting points, Si and Ge typically require the use of catalyst nanoparticles to facilitate anisotropic growth. A wide range of metal catalysts have been used from noble metals (Au,[8, 9] Ag,[10]), transition metals (Cu,[11-13] Ni,[14-16] Fe[17]) to the low melting point p-block metals (Sn,[18-20] Bi[21, 22] and In[23-26]). The most successful route employs chemical vapour deposition (CVD) where either a liquid (VLS) or solid (VSS) catalyst seed acts as a sink for gaseous precursors from the vapour phase leading to the nucleation of a solid NW at the interface between the seed and the substrate. The progress in understanding of these growth mechanisms has allowed a range of very complex NW morphologies from core/shell[27, 28] to linear heterostructures[29-32] to be obtained by tuning the composition of the reactant vapour and reaction time. Strategies to simplify the system by replacing the highly reactive gaseous precursors with liquid analogues are attractive as they potentially allow for greater scalability with less energy intensive processes.[33-36] Single crystal NWs of both Si and Ge have been nucleated in supercritical solvents using a variety of precursors.[37-39] In non-pressurised wet chemical systems, Ge wires can be generated in solution using high boiling point solvents (HBS),[35, 40] however, as Si requires higher nucleation temperatures compared to Ge, Si NW formation typically requires the use of extremely reactive precursors (e.g. trisilane[21]). A constraint of these solvent based approaches is the reduction in the achievable complexity in the resultant NWs as the systems are typically not suitably flexible to allow instantaneous changes in the source material to switch from Si growth to Ge growth in a single NW.

In our research we have developed a solvent vapor growth (SVG) system[36, 41] that is a wet-chemical, glassware based approach, that allows for much greater flexibility and hence complexity in NW formation. The substrates are placed in the reaction flask with the growth zone occurring above the liquid meniscus of a HBS at reflux (i.e. within the HBS vapour). The liquid precursors of Si and Ge are injected into the vapour zone allowing NW growth *via* a range of catalytic approaches. NW growth has been shown by self-induced solid phase seeding from bulk metal substrates[12, 42] and also *via* VLS mechanism from evaporated catalytic layers that convert to discrete seeds under thermal anneal. The method allows the formation of both Si and Ge NWs using VLS (Sn[20] and In seeds[26]) and VSS catalytic approaches (using bulk Cu[12, 42]) and has also been shown to allow seed-free Ge NW growth[41] directly from glass/Pyrex flask walls.[41, 43] The use of p-block metals (e.g In and Sn) is interesting as although these have low melting points and a very low solubility for Si and Ge in the liquid eutectic, they allow for a high density of NW formation suitable for Li-ion alloying anodes.[44] In a preliminary report, we demonstrated the adaptability of this SVG system with Sn as the catalyst seed to allow the formation of axial heterostructure NWs (HNWs) by switching the liquid precursor from Si to Ge by sequential injection.[45] This growth approach combined with the low solubilities of Si and Ge in the catalyst led to a marked reduction of the interfacial heterogeneity between the Si and Ge segment (compared to conventionally catalysed HNW) in single HNWs with a near atomic abruptness verified through the use of aberration corrected microscopy and atomic level electron energy loss spectroscopy. Here, we demonstrate the versatility of this system by obtaining control over the respective segment lengths of Si and Ge in the heterostructure. Further we extend the heterostructure formation to In metal seeds and compare the NW morphologies to Sn-seeded analogues. Finally we show and analyse the formation of Si-Ge-Si_xGe_y HNWs through a third sequential injection.

Experimental

All chemicals were used as received unless otherwise stated. Squalane (99%) and phenylsilane (PS) (97 %) were received from Aldrich. Precursors diphenylgermane (DPG) (97%), and triphenylgermane (TPG) (>95%), were supplied by Fluorochem. All syntheses were carried out using long neck Pyrex round-bottomed flasks by Technical Glass Products Inc. All experiments were conducted using an Applied Test Systems Inc. Model 3210, 3-zone heating furnace, which was regulated the temperature of each reaction within the round bottomed flasks to an accuracy of +/- 5°C.

Substrate preparation and post synthetic treatment.

Reaction substrates (stainless steel (SS) foil) we prepared by evaporating 20 nm thick layers 99.99% Sn/In (Kurt J Lesker company) in a glovebox based evaporation unit. The substrates were stored in an Ar glovebox prior to reactions and contact with O_2 was minimized. After synthesis, the substrates were simply rinsed with toluene, to remove excess solvent, and dried using a nitrogen line. No additional cleaning steps were required.

Reaction setup

NW growth reactions were carried out in the SVG system described in previous reports.[26, 36, 41, 45] The system encompasses a custom made Pyrex round bottomed flask within a three zone furnace. The flask was connected to a Schlenk line to allow both vacuum and Ar lines for the flask. The reactions were carried out within the vapour phase of the HBS squalane. 10 ml of squalane was loaded into the long necked round bottomed flask along with the catalyst (either Sn or In) covered substrate. The furnace was ramped to 110 ° C, held at this temperature and degassed under vacuum for 30 min. Following this period, the reaction times and precursors were varied depending on the NWs which were to be grown. The growth conditions for Si

and Ge NWs (using Sn[20] and In[26]) and Sn catalyzed Si/Ge HNWs[45] are presented in previously published reports.

For the more complex double junction NWs, the system was ramped to 450 °C (under Ar) and 0.5 ml phenylsilane was injected and reacted for 45 minutes (1st segment). The temperature was ramped down to 430 °C and 0.2 ml TPG (0.33 g TPG/1 ml squalane – stock solution) was injected with the reaction allowed to proceed for 5 min (2nd segment). To grow the final segment, the system was ramped up to 450 °C and 0.5 ml PS was injected. This segment was allowed to grow for another 45 min (3rd segment). Following this growth time, the furnace was opened, the temperature controller was switched off and the flask was allowed to cool to room temperature.

Analysis

SEM analysis was performed on a Hitachi SU-70 system operating between 3 and 20 kV. The Sn and In substrates were untreated prior to SEM analysis. For TEM analysis, the NWs were removed from the growth substrates through the use of a sonic bath. TEM analysis was conducted using a 200 kV JEOL JEM-2100F field emission microscope equipped with a Gatan Ultrascan CCD camera and EDAX Genesis EDS detector. EDX analysis of the NWs was conducted on Au TEM grids. XRD analysis was conducted using a PANalytical X'Pert PRO MRD instrument with a Cu-K_α radiation source (λ= 1.5418 Å) and an X'celerator detector.

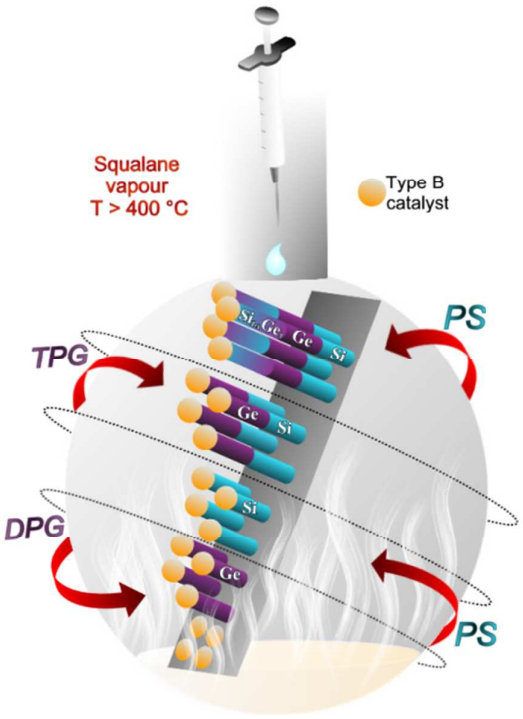

Figure 1. Schematic depiction of the SVG system used for NW synthesis.

Results and discussion:

The SVG method for NW formation is depicted schematically in Figure 1. The glassware based approach is a one-pot system suited to the growth of a range of Ge and Si NW structures. The growth substrates (SS) were coated with thermally evaporated metals (either In or Sn) which act as NW growth catalysts. The NW structures which can be formed using this approach are depicted in the schematic along with the progression of precursor injections required to induce the growth of each of the HNWs. As Si is less reactive than Ge, the growth of the Si segment first is advantageous as the transition to Ge growth is instantaneous once introduced into the system. It is possible to accurately tune the respective segment lengths by

controlling the growth of each segment even though the growth kinetics for Si growth is much slower than Ge. In our observations, the growth rate for Sn seeded Ge at 420 °C is approximately 3 times the growth rate for Si at 450 °C allowing for accurate control as a function of time and temperature. Obtaining HNWs with approximately similar Si and Ge segment lengths (Figure 2 a) could therefore be obtained by a Si reaction time of 30 minutes followed by a Ge reaction time of 10 minutes. The temperature perturbation is also aided by the injection of the cold volume of liquid into the flask. Figure 2b shows Si/Ge HNWs with a short Ge section and much longer Si segment formed by growing the Si segment for 60 minutes with the Ge segment for only 2 minutes in addition to lowering the temperature by 30 °C. These results show the tunability of the growth method and through further control over the precursor reactivity and dwell times, it is likely that even more precise control over the segment lengths could be achieved.

The 'bulge' at the interface of the Ge/Si HNWs is largely due to the different wetting behaviour of Sn with Si and Ge.[24, 46, 47] This is reflected in the seed size to NW diameter ratio of discrete wires seeded from Sn (Figure S1) which were found to be approximately 2.25:1 and 1.75:1 for Ge and Si respectively. In comparison, the archetypal catalyst material Au (which also has a much higher % of Si and Ge in the respective eutectic alloys) typically allows for a ≈1:1 ratio of seed size to NW diameter.[48] It is therefore possible using catalysts such as Sn and In to form NWs with smaller diameters for a given seed size. Thus, the larger seeds obtained by thermally annealing evaporated metal layer presented here are suitable for the formation of NWs with diameters well below 100 nm, negating the need for discrete seed formation *ex-situ*. These observations fit well with previous work by Gamalski et al. who showed that alloying Au with Ga (which has similar wetting behaviour with Si and Ge) resulted in an increase in the size of the interfacial bulged region.[49] They also observed an

improvement in compositional abruptness which fits very well with our findings that the use of pure Sn leads to an atomically abrupt interface.[45]

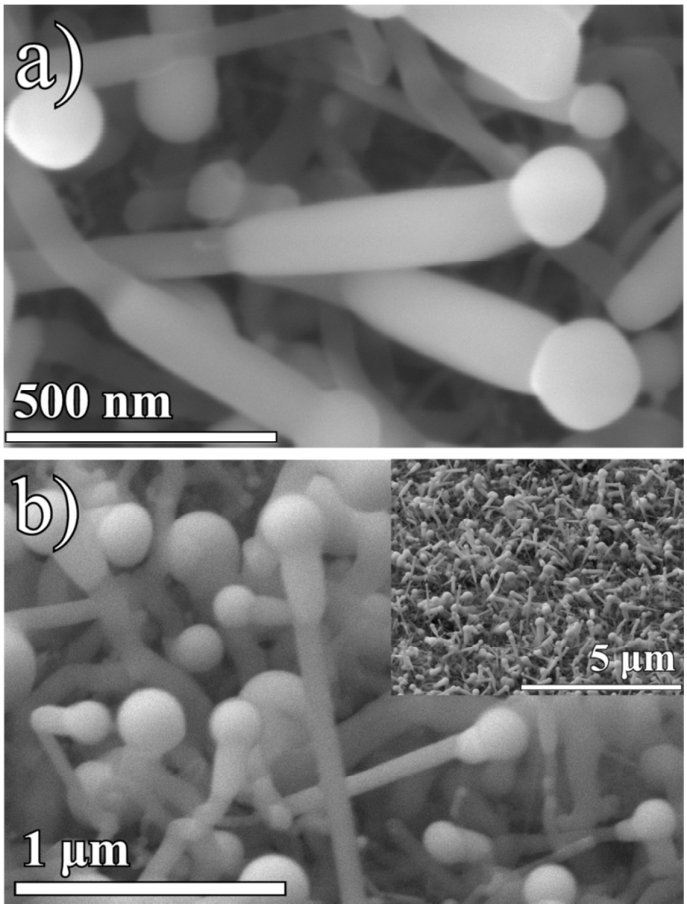

Figure 2. SEM analysis of Sn catalysed Si-Ge NWs with a) a Si reaction time of 30 min followed by a Ge reaction time of 10 min. b) Si reaction time of 60 min followed by a Ge reaction time of 2 min (inset shows the density of the NWs on the SS substrate).

Si/Ge HNW grown from In and length variation

The use of In as a catalyst material for Si/Ge HNW growth was also investigated. In Figure 3 a) the SEM image shows Si/Ge HNWs grown using an In catalyst where a narrower Si segment and broader Ge segment are clearly visible in the linear heterostructure. The In seed to Si NW diameter ratios are slightly larger than those observed for Sn typically at 3.5:1 for Si (consistent with our previous results[26]) while the In/Ge ratio is similar to that of In/Si at

1.7:1 (Figure S2). EDX analysis (Figure 3b) confirmed the presence of In, Si and Ge but also a signal for O which is due to partial oxidation of the In catalysts after exposure to air (Figure S3). The TEM and DFSTEM images of single HNWs shown in Figure 3 c) and Figure 3 d) respectively show the effect of the different wetting behaviour on the respective NW diameters and the extent of tapering at the interface. Remarkably, despite a 400 % expansion of the interfacial growth zone on transitioning from Si to Ge, the interfaces remain intact across the entire NW batch. This diameter ratio is strongly influenced by the contact angle of the liquid catalyst droplet on the evolving NW. For example, it has been shown that In possesses a much larger contact angle on Si than Au does, which leads to much smaller NWs being formed for a given catalyst size from In.[50] DFSTEM of an In seeded (Figure 3 d) and the corresponding EDX line scan (e) confirm the abrupt compositional change from the In catalyst to the Ge segment and finally, the Si segment. The line profile also shows a lack of significant Si in the Ge section and vice versa. The compositional abruptness of the In catalyzed Si/Ge HNW is similar to the profile measured for the Sn catalyzed Si/Ge NWs using the same STEM/EDX instrument (Figure S4). Again, it is worth noting that the Sn catalyzed Si/Ge NWs have been shown to have extremely sharp heterointerfaces by aberration corrected STEM/EELS analysis and it is thus likely that the In possess a sharper Si/Ge interface than suggested by the EDX line scan in Figure 3 e).[45] While the EDX signal for In is low throughout the measured HNW, is it possible that In may be incorporated in the HNWs below the detection limit of the instrument.

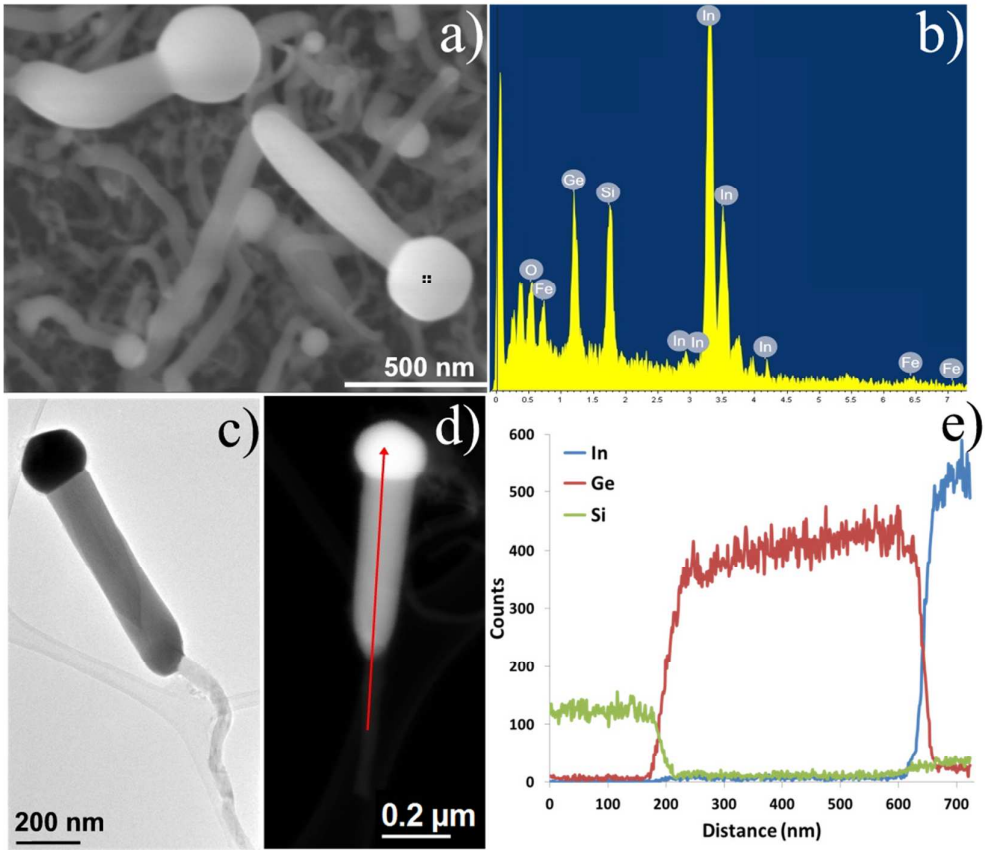

Figure 3. a) SEM analysis of In catalyzed Si-Ge NWs. b) Point EDX analysis of the nanowire highlighted in a). c) BFTEM and d) DFSTEM of an In seeded Si-Ge NW. e) EDX line scan of the NW highlighted in d)

The lengths of the Si and Ge segments in the HNWs seeded using In could also be controlled by varying the reaction parameters (Figure S5). In the case of In, the length dependence on growth time was 15 times faster for Ge in comparison to Si at respective growth temperatures of 450 °C and 420 °C, alowing similar segment lengths of 1 µm after 30 minutes of Si growth followed by 2 minutes of Ge growth. It was noted that elemental Ge NWs were formed in the solution portion of the SVG system as a byproduct of Si/Ge HNW syntheses (Figure S6). Otherwise, no NW growth was noted in the HBS solution. The growth of Ge NWs in the solution phase in this case is due to the action of PS (used for the Si/Ge HNW growth) which increases the reactivity of the DPG precursor and thus allows

Ge NW growth in the solution phase.[51]

To further investigate the role of catalyst materials with similar eutetic compositions to In and Sn for Si, Ge and HNW growth, the use of Bi was also investigated. In contrast to reactions conducted using In and Sn, it was found that only Ge NWs could succesfully be formed using Bi as a catalyst materials (Figure S7). While Bi has been used in alternative approaches for Si NW catalysis[21, 22] it typically requires the extremely reactive precursor trisilane or plasma enhanced CVD to enable NW growth. The lack of Si growth (and thus HNW growth) from Bi in our system is likely due to a combination of the lesser reactivity of our precursor compared to the aforementioned reports and the low surface tension of Bi on Si as calculated by Nebol'sin.[52] Schmidt et al. reviewed the suitability of a range of low solubility catalyst materials (such as Sn, In, Ga and Bi) and attributed the instability of Bi to a combination of low Si solubility as well as the low surface tension of Bi in a metal-silicon system (0.355 J/m2 at 800 K, compared to 0.910 J/m2 at 1400 K for Au according to the Nebol'sin criterion).[53]

Growth of multistructure Si/ Ge/ $Si_{1-x}Ge_x$ HNWs from Sn and In

The growth of more complex Si/ Ge/ $Si_{1-x}Ge_x$ HNWs was also achieved using the one-pot, SVG system. Following the growth of Si/Ge as described above from Sn catalysts, the reaction temperature was again raised to 450 °C and the PS precursor was introduced (i.e. a third growth step). SEM images (Figure 4 a, b) of the HNWs confirmed the presence of two heterojunctions in the NW structures. The DFSTEM image in Figure 4 c) shows a clean Si/Ge heterojunction (magnified in Figure 4 d) consistent with the previous Si/Ge HNWs presented and a more complex heterojuntion grown in the third growth step (magnified in Figure 4 e). It can be seen that there are two crystallographic defects which begin in the Si segment of the HNW in Figure 4 d) which continue into the Ge segment of the HNW. The prevalence of defects in the HNWs and transference from the Si NW segment to the Ge NW

segment were previously noted for Sn catalyzed HNWs in this system.[45]

The chemical composition of the complex third segment was probed using EDX analysis (Figure 4 f). From the left of the EDX profile, it can be seen that the scan starts with the pure Ge segment grown in step two of the reaction. Overall it can be seen that this third segment is composed of a Si_xGe_y alloy with varying degrees of Si and Ge throughout. This is to be expected given the fact that there is still residual Ge monomer in the growth system once the Si precursor has been injected. The increased temperature required for the growth of the Si segment compared to the Ge (450 °C compared to 430 °C) likely hastens the decomposition of the remaining Ge precursor resulting in local fluctuations in the Ge and Si content. This compositional variation is also influenced by the activation of the phenyl containing Ge precursor by the presence of phenylsilane previously reported by Lu et al.[51] Tapering is again evident at the heterojunction between the pure Ge segment and the Si_xGe_y portion which is due to a variation of the seed/NW contact angle with varying composition of the evolving HNW.

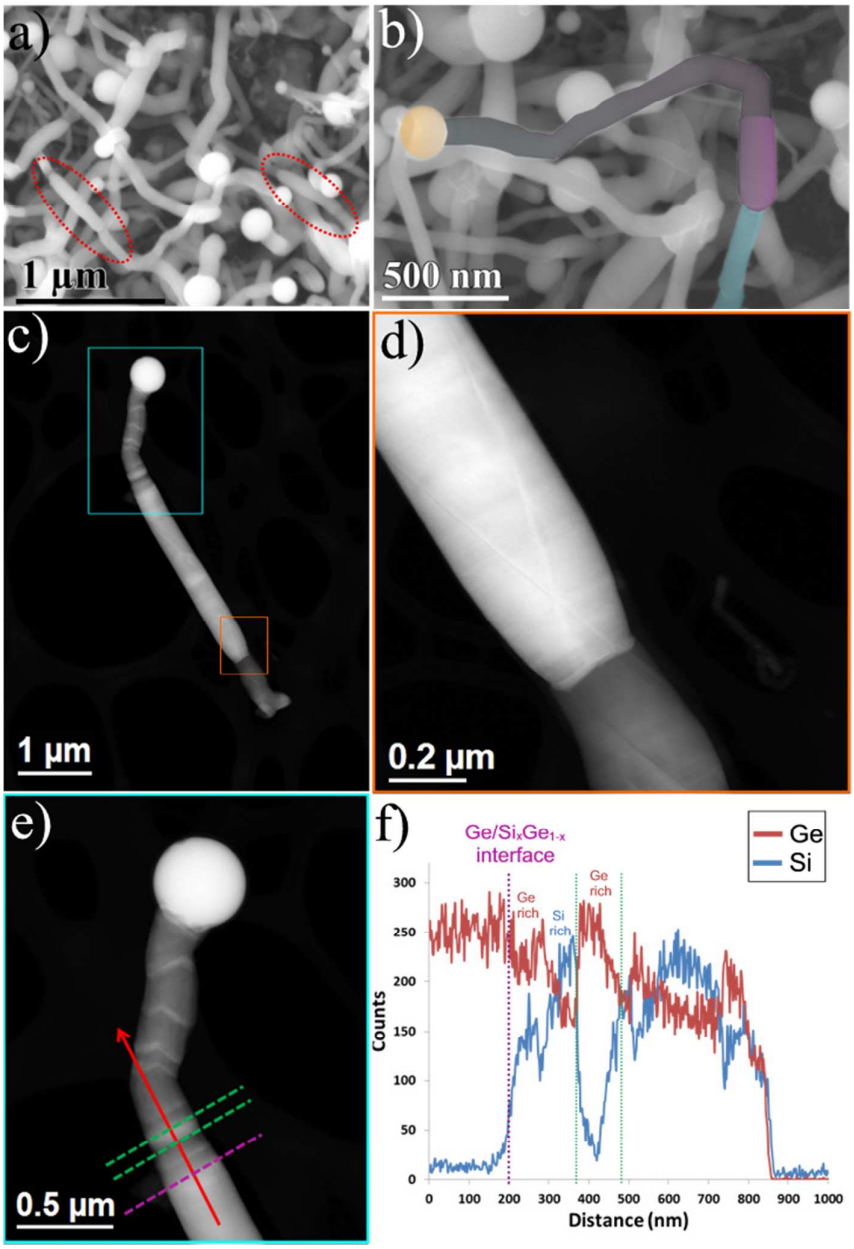

Figure 4. a) Low magnification SEM image showing the as-synthesized Sn catalyzed triple segmented NWs. Three NW segments are highlighted by red dotted circles. b) A higher magnification SEM image showing an artificially coloured Sn catalyzed triple segmented NW. c) LR-DFSTEM of the NW showing the three main NW segments and spherical Sn seed. d) Higher magnification DFSTEM image of the Ge/Si interface highlighted in c) (orange). e) DFSTEM image of the third NW segment (highlighted in blue in c)) and corresponding EDX line scan in f).

In was also probed as a catalyst material for Si/Ge/Si NW growth by employing an additional Si growth section (similar to the approach adopted for Sn). In Figure 5 a) and b) SEM images of the HNWs with three segments containing different compositions grown using In are presented. There is obvious tapering between the Si and Ge as seen in the DFSTEM image in Figure 5 c). The Z-contrast difference between the Si, Ge and Si_xGe_y segment in the In catalyzed HNW are clear in this image while the diameters of the various segments again correlate with the observed diameters for the elemental NWs (i.e. Ge>Si_xGe_y>Si). The mixed composition of the third segment in the NW was again confirmed through the use of EDX (Figure 5 d)) analysis which showed a more uniform composition of Si and Ge in this segment compared to those grown using Sn as the catalyst. The TEM image in Figure 5 e) shows the nature of the interface between the pure Si segment and the Ge portion for the same NW with the inset FFT patterns indexed for Si (i) and Ge (ii). The corresponding EDX line profile Figure 5 f) again shows an abrupt interface between the Si and Ge and low background signal from the alternate element in each segment.

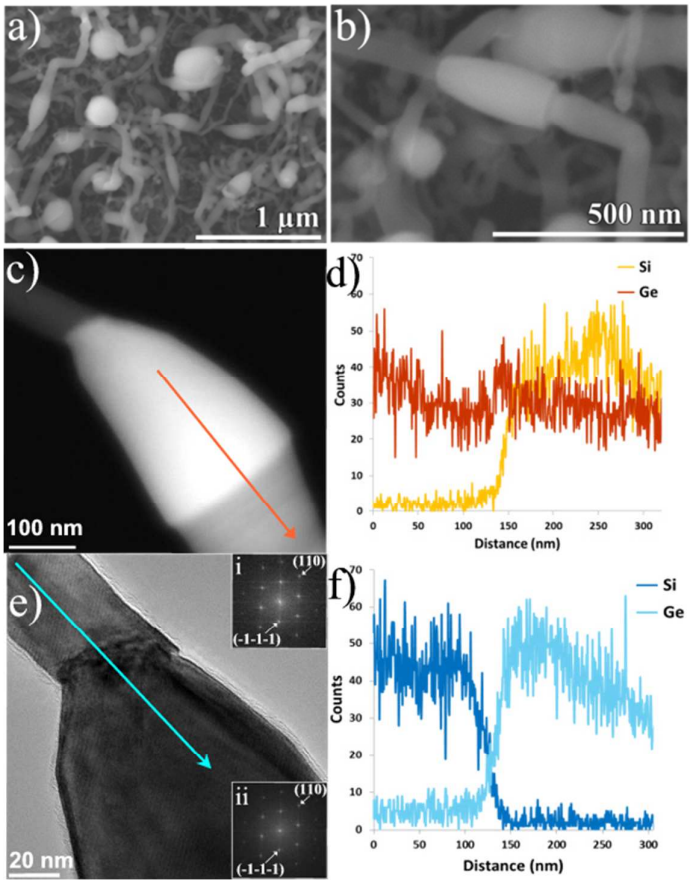

Figure 5. a),b) SEM images of In catalysed triple segmented NWs. c) DFSTEM image of Si/ Ge/ Si_xGe_y HNW with arrow indicating the direction of the EDX line profile shown in d). e) TEM image with inset FFTs of Si (i) and Ge (ii). The arrow on the image shows the direction of the EDX line scan in f).

Conclusions

In conclusion, we have examined the use of Type B metal catalysts for Si, Ge and complex Si/Ge axial heterostructures within a one-pot SVG system. The impact of the catalyst material investigated was probed with a direct comparison made between the use of Sn and In. The successful growth of Si/Ge HNWs using an In catalyst illustrated the versatility of low solubility metal catalyst materials. Tapering was noted between the sections of the HNWs which was caused by the different wetting behaviours of the different Type B catalysts on the Si, Ge and Si_xGe_y segments. The formation of mixed Si/Ge segments was due to residual Ge in the growth system after the introduction of the Si precursor.

Acknowledgements

This work was supported principally by Science Foundation Ireland (SFI) under the Principal Investigator Program (Contract No. 11PI-1148) and was conducted under the framework of the Irish Government's Programme for Research in Third Level Institutions Cycle 5, National Development Plan 2007-2013 with the assistance of the European Regional Development Fund. Support of Intel Ireland is further acknowledged.

References:

1. Cui, Y.; Zhong, Z.; Wang, D.; Wang, W. U.; Lieber, C. M. *Nano Lett.* **2003,** 3, (2), 149-152.
2. Xiang, J.; Lu, W.; Hu, Y.; Wu, Y.; Yan, H.; Lieber, C. M. *Nature* **2006,** 441, (7092), 489-493.
3. Garnett, E. C.; Yang, P. *J. Am. Chem. Soc.* **2008,** 130, (29), 9224-9225.
4. Garnett, E.; Yang, P. *Nano Lett.* **2010,** 10, (3), 1082-1087.
5. Chan, C. K.; Zhang, X. F.; Cui, Y. *Nano Lett.* **2007,** 8, (1), 307-309.
6. Chan, C. K.; Peng, H.; Liu, G.; McIlwrath, K.; Zhang, X. F.; Huggins, R. A.; Cui, Y. *Nat Nano* **2008,** 3, (1), 31-35.
7. Chockla, A. M.; Harris, J. T.; Akhavan, V. A.; Bogart, T. D.; Holmberg, V. C.; Steinhagen, C.; Mullins, C. B.; Stevenson, K. J.; Korgel, B. A. *J. Am. Chem. Soc.* **2011,** 133, (51), 20914-20921.
8. Hanrath, T.; Korgel, B. A. *J. Am. Chem. Soc.* **2002,** 124, (7), 1424-1429.
9. Collins, G.; Kolesìnik, M.; Krsticì , V.; Holmes, J. D. *Chem. Mater.* **2011,** 22, (18), 5235-5243.
10. Wittemann, J. V.; Munchgesang, W.; Senz, S.; Schmidt, V. *J. Appl. Phys.* **2010,** 107, (9), 3.
11. Kang, K.; Kim, D. A.; Lee, H.-S.; Kim, C.-J.; Yang, J.-E.; Jo, M.-H. *Adv. Mater.* **2008,** 20, (24), 4684-4690.
12. Geaney, H.; Dickinson, C.; Barrett, C. A.; Ryan, K. M. *Chem. Mater.* **2011,** 23, (21), 4838-4843.
13. Richards, B. T.; Gaskey, B.; Levin, B. D. A.; Whitham, K.; Muller, D.; Hanrath, T. *J. Mater. Chem. C* **2014,** 2, (10), 1869-1878.
14. Tuan, H.-Y.; Lee, D. C.; Hanrath, T.; Korgel, B. A. *Chem. Mater.* **2005,** 17, (23), 5705-5711.
15. Tuan, H.-Y.; Lee, D. C.; Hanrath, T.; Korgel, B. A. *Nano Lett.* **2005,** 5, (4), 681-684.
16. Barth, S.; Kolesìnik, M. M.; Donegan, K.; Krsticì , V.; Holmes, J. D. *Chem. Mater.* **2011**, 23 14, 3335–3340
17. Mathur, S.; Shen, H.; Sivakov, V.; Werner, U. *Chem. Mater.* **2004,** 16, (12), 2449-2456.
18. Rathi, S. J.; Jariwala, B. N.; Beach, J. D.; Stradins, P.; Taylor, P. C.; Weng, X.; Ke, Y.; Redwing, J. M.; Agarwal, S.; Collins, R. T. *J. Phys. Chem. C* **2011,** 115, (10), 3833-3839.
19. Chockla, A. M.; Klavetter, K.; Mullins, C. B.; Korgel, B. A. *Chemistry of Materials* **2012**. 24, 19, 3738–3745
20. Mullane, E.; Kennedy, T.; Geaney, H.; Dickinson, C.; Ryan, K. M. *Chem. Mater.* **2013,** 25, (9), 1816-1822.
21. Heitsch, A. T.; Fanfair, D. D.; Tuan, H.-Y.; Korgel, B. A. *J. Am. Chem. Soc.* **2008,** 130, (16), 5436-5437.
22. Yu, L.; Fortuna, F.; O'Donnell, B.; Jeon, T.; Foldyna, M.; Picardi, G.; Roca i Cabarrocas, P. *Nano Lett.* **2012,** 12, (8), 4153-4158.
23. P. J. Alet, L. Y., G. Patriarche, S. Palacin and P. R. i Cabarrocas. *J. Mater. Chem.* **2008,** 18, 5187-5189.
24. Wang, Z. W.; Li, Z. Y. *Nano Lett.* **2009,** 9, (4), 1467-1471.
25. Zardo, I.; Conesa-Boj, S.; Estrade, S.; Yu, L.; Peiro, F.; Cabarrocas, P. R. I.; Morante, J. R.; Arbiol, J.; Morral, A. F. I. *Appl.Phys. a-Materials Science & Processing* **2010,** 100, (1), 287-296.
26. Geaney, H.; Kennedy, T.; Dickinson, C.; Mullane, E.; Singh, A.; Laffir, F.; Ryan, K. M. *Chem. Mater.* **2012,** 24, (11), 2204-2210.

27. Lauhon, L. J.; Gudiksen, M. S.; Wang, D.; Lieber, C. M. *Nature* **2002,** 420, (6911), 57-61.
28. Liang, G.; Xiang, J.; Kharche, N.; Klimeck, G.; Lieber, C. M.; Lundstrom, M. *Nano Lett.* **2007,** 7, (3), 642-646.
29. Wu, Y.; Fan, R.; Yang, P. *Nano Lett.* **2002,** 2, (2), 83-86.
30. Wen, C.-Y.; Reuter, M. C.; Bruley, J.; Tersoff, J.; Kodambaka, S.; Stach, E. A.; Ross, F. M. *Science* **2009,** 326, (5957), 1247-1250.
31. Amato, M.; Palummo, M.; Rurali, R.; Ossicini, S. *Chem. Rev.* **2013,** 114, (2), 1371-1412.
32. Rurali, R.; Cartoixà, X.; Colombo, L. *Phys. Rev. B* **2014,** 90, (4), 041408.
33. Holmes, J. D.; Johnston, K. P.; Doty, R. C.; Korgel, B. A. *Science* **2000,** 287, (5457), 1471-1473.
34. Lu, X.; Hanrath, T.; Johnston, K. P.; Korgel, B. A. *Nano Lett.* **2002,** 3, (1), 93-99.
35. Chockla, A. M.; Korgel, B. A. *J. Mater. Chem.* **2009,** 19, (7), 996-1001.
36. Geaney, H.; Mullane, E.; Ryan, K. M. *J. Mater. Chem. C* **2013,** 1, (33), 4996-5007.
37. Hanrath, T.; Korgel, B. A. *Adv. Mater.* **2003,** 15, (5), 437-440.
38. Lu, X.; Ziegler, K. J.; Ghezelbash, A.; Johnston, K. P.; Korgel, B. A. *Nano Lett.* **2004,** 4, (5), 969-974.
39. Barrett, C. A.; Gunning, R. D.; Hantschel, T.; Arstila, K.; O'Sullivan, C.; Geaney, H.; Ryan, K. M. *J. Mater. Chem.* **2010,** 20, (1), 135-144.
40. Chockla, A. M.; Harris, J. T.; Korgel, B. A. *Chem. Mater.* **2011,** 23, (7), 1964-1970.
41. Barrett, C. A.; Geaney, H.; Gunning, R. D.; Laffir, F. R.; Ryan, K. M. *Chem. Commun.* **2011,** 47, (13), 3843-3845.
42. Geaney, H.; Dickinson, C.; O'Dwyer, C.; Mullane, E.; Singh, A.; Ryan, K. M. *Chem. Mater.* **2012,** 24, (22), 4319-4325.
43. Geaney, H.; Dickinson, C.; Weng, W.; Kiely, C. J.; Barrett, C. A.; Gunning, R. D.; Ryan, K. M. *Cryst. Growth & Des.* **2011,** 11, (7), 3266-3272.
44. Kennedy, T.; Mullane, E.; Geaney, H.; Osiak, M.; O'Dwyer, C.; Ryan, K. M. *Nano Lett.* **2014,** 14, (2), 716-723.
45. Geaney, H.; Mullane, E.; Ramasse, Q. M.; Ryan, K. M. *Nano Lett.* **2013,** 13, (4), 1675-1680.
46. Iacopi, F.; Richard, O.; Eichhammer, Y.; Bender, H.; Vereecken, P. M.; Gendt, S. D.; Heyns, M. *Electrochem. Solid-State Lett.* **2008,** 11, (9), K98-K100.
47. Yu, L. W.; O'Donnell, B.; Alet, P. J.; Conesa-Boj, S.; Peiro, F.; Arbiol, J.; Cabarrocas, P. I. R. *Nanotechnol.* **2009,** 20, (22), 5.
48. Wu, Y.; Cui, Y.; Huynh, L.; Barrelet, C. J.; Bell, D. C.; Lieber, C. M. *Nano Lett.* **2004,** 4, (3), 433-436.
49. Gamalski, A. D.; Perea, D. E.; Yoo, J.; Li, N.; Olszta, M. J.; Colby, R.; Schreiber, D. K.; Ducati, C.; Picraux, S. T.; Hofmann, S. *ACS Nano* **2013,** 7, (9), 7689-7697.
50. Mattila, M.; Hakkarainen, T.; Lipsanen, H.; Jiang, H.; Kauppinen, E. *Appl.Phys. Lett.* **2006,** 89, (6), 063119.
51. Lu, X.; Harris, J. T.; Villarreal, J. E.; Chockla, A. M.; Korgel, B. A. *Chem. Mater.* **2013,** 25, (10), 2172-2177.
52. Nebol'sin, V. A.; Shchetinin, A. A. *Inorg. Mater.* **2003,** 39, (9), 899-903.
53. Schmidt, V.; Wittemann, J. V.; Gosele, U. *Chem. Rev.* **2010,** 110, (1), 361-388.